IEEE Access
Multidisciplinary ⋮ Rapid Review ⋮ Open Access Journal

Received August 1, 2020, accepted September 7, 2020, date of publication September 10, 2020, date of current version September 24, 2020.

Digital Object Identifier 10.1109/ACCESS.2020.3023133

1.6-Octave Coherent OAM Supercontinuum Generation in As_2S_3 Photonic Crystal Fiber

WENPU GENG[1], CHANGJING BAO[2], (Member, IEEE), YUXI FANG[1], YINGNING WANG[1], YIQIAO LI[1], ZHI WANG[1], YAN-GE LIU[1], HAO HUANG[2], (Member, IEEE), YONGXIONG REN[2], (Member, IEEE), ZHONGQI PAN[3], (Senior Member, IEEE), AND YANG YUE[1], (Member, IEEE)

[1]Institute of Modern Optics, Nankai University, Tianjin 300350, China
[2]Department of Electrical Engineering, University of Southern California, Los Angeles, CA 90089, USA
[3]Department of Electrical and Computer Engineering, University of Louisiana at Lafayette, Lafayette, LA 70504, USA

Corresponding author: Yang Yue (yueyang@nankai.edu.cn)

This work was supported in part by the National Key Research and Development Program of China under Grant 2019YFB1803700, in part by the National Natural Science Foundation of China (NSFC) under Grant 11774181 and Grant 61775107, in part by the Key Technologies Research and Development Program of Tianjin under Grant 20YFZCGX00440, and in part by the Fundamental Research Funds for the Central Universities, Nankai University, under Grant 63201178 and Grant 63191511.

ABSTRACT We design and simulate an all-normal dispersion arsenic trisulfide (As_2S_3) photonic crystal fiber (PCF) with high nonlinearity to enable a flat and coherent orbital angular momentum (OAM) supercontinuum (SC) generation. The photonic crystal fiber features a near-zero and flat negative dispersion with variation between −96.5 and −36.5 ps/(nm·km) over a 940-nm wavelength range from 1740 to 2680 nm. A 1946-nm supercontinuum forms from 959 to 2905 nm at −20 dB level which covers a 1.6-octave bandwidth, by launching a 100-fs 5-kW chirp-free hyperbolic secant pulse with wavelength at 2000 nm into a 1.0-cm designed fiber. The generated supercontinuum of the other two vortex modes (TE_{01} and TM_{01}) can cover more than two octaves by optimizing the proposed fiber structures. The coherence of the generated supercontinuum of the three modes all shows nearly perfect property over the whole bandwidth. In general, we found that the designed ring-core As_2S_3 PCF with all-normal dispersion could be used for broadband coherent supercontinuum generation of various vortex modes.

INDEX TERMS Optical vortices, photonic crystal fibers, supercontinuum.

I. INTRODUCTION

Light-carrying orbital angular momentum (OAM) has recently drawn extensive attention from researchers due to its great value in classical and quantum communications [1]–[3], stimulated emission depletion (STED) super-resolution microscopy [4], sensing [5], and laser material processing [6]. The OAM beams feature with helical phase fronts of $\exp(il\phi)$, where l and ϕ represent the topological charge and azimuthal angle, respectively [7]. As a result of the intrinsic orthogonality among OAM modes with different l values, they can be used as a modal basis in the mode-division multiplexing (MDM) optical communications systems. In order to better propagate the OAM modes, one needs to avoid the degeneracy of the vortex-like modes. Consequently, the fiber is usually designed with a ring-shaped high-index profile, and large effective refractive index contrast ($\Delta n_{eff} > 10^{-4}$) between different modes can be achieved [8]–[10].

Over the past two decades, the optical fiber community has paid significant attention to photonic crystal fiber (PCF), which enables many novel devices and applications. Its special and adjustable structure empowers several unique properties that could not be easily realized by conventional fibers, such as endlessly single-mode guiding, high birefringence, and controllable nonlinearity [11]–[17]. One of the fundamental advantages of PCF is its flexible dispersion engineering, which could potentially enable broadband supercontinuum (SC) generation.

Supercontinuum with a broad bandwidth and high coherence is of vital importance for many applications, such as optical coherence tomography, optical sensing, and optical frequency comb [18]–[21]. Chalcogenide materials are very promising for nonlinear applications due to its high nonlinear refractive index. By leveraging this material, chalcogenide PCF could achieve both the high nonlinearity and near-zero

The associate editor coordinating the review of this manuscript and approving it for publication was Rene Essiambre.

flat dispersion, which play critical roles in efficient supercontinuum generation over broad bandwidth [22], [23]. Some simulation investigations and experimental demonstrations [24], [25] have further shown that PCF with all-normal dispersion can be used to generate a flat and highly coherent supercontinuum by completely eliminating the modulation instability and the influences of the soliton [26].

In this work, we design and optimize an As_2S_3 ring-core PCF with all-normal dispersion that supports OAM modes. The PCF features a near-zero and flat negative dispersion with the variation from −96.5 to −36.5 ps/(nm·km) over a 940-nm bandwidth from 1740 to 2680 nm. A 1946-nm supercontinuum is formed from 959 to 2905 nm at −20 dB level, which covers a 1.6-octave bandwidth, when a 100-fs 5-kW chirp-free hyperbolic secant pulse is launched into a 1.0-cm designed fiber. Furthermore, we investigated the SC generation of the TE_{01} and TM_{01} modes with all-normal dispersion by optimizing the fiber structure parameters. With a 100-fs 8-kW pump pulse at the wavelength of 2500 nm coupled into a 2-mm optimized PCF, we achieved a supercontinuum of the TE_{01} mode covering over 2-octave bandwidth from 819 to 3440 nm at −30 dB. Additionally, by launching a 100-fs 20-kW pulse into a 2-mm long PCF, the supercontinuum of the TM_{01} mode can be generated from 849 to 3504 nm at −20 dB, which is also larger than two octaves. The generated supercontinua show nearly perfect coherence property over the whole bandwidth.

II. RING PCF DESIGN

Figure 1(a) depicts the concept diagram of OAM supercontinuum generation by using the proposed ring-core As_2S_3 PCF. As a short pulse launched into the proposed fiber, due to the interaction between the normal dispersion and nonlinear effects along the propagation, a flat and highly coherent SC is generated. The PCF has an air hole in the center. Its cladding consists of seven layers of air holes arranged in a regular hexagonal order, as displayed in Fig. 1(b). The geometric parameters of the fiber are set as follows: r_0 is the radius of the central air hole, r_2 to r_8 are the radii of the air holes in the cladding, and d is the air hole pitch between the centers of proximal holes. The material of the background cladding is As_2S_3. Using a full-vector finite-element mode solver and applying the perfectly matched boundary layer, we can obtain the electromagnetic field distributions of the vortex modes (TE_{01}, TM_{01}, $HE_{2,1}^{even}$ and $HE_{2,1}^{odd}$) in the ring-core PCF (d = 0.4 μm, r_0 = 0.17 μm, r_2 = 0.1 μm, r_3 = 0.15 μm, r_4 = 0.18 μm, r_5 to r_8 = 0.19 μm) at 2000 nm as illustrated in Fig. 1. (c). Furthermore, $OAM_{1,1}$ mode can be supported in the PCF with the combination of its two eigenmodes ($OAM_{1,1} = HE_{2,1}^{even} + i \times HE_{2,1}^{odd}$).

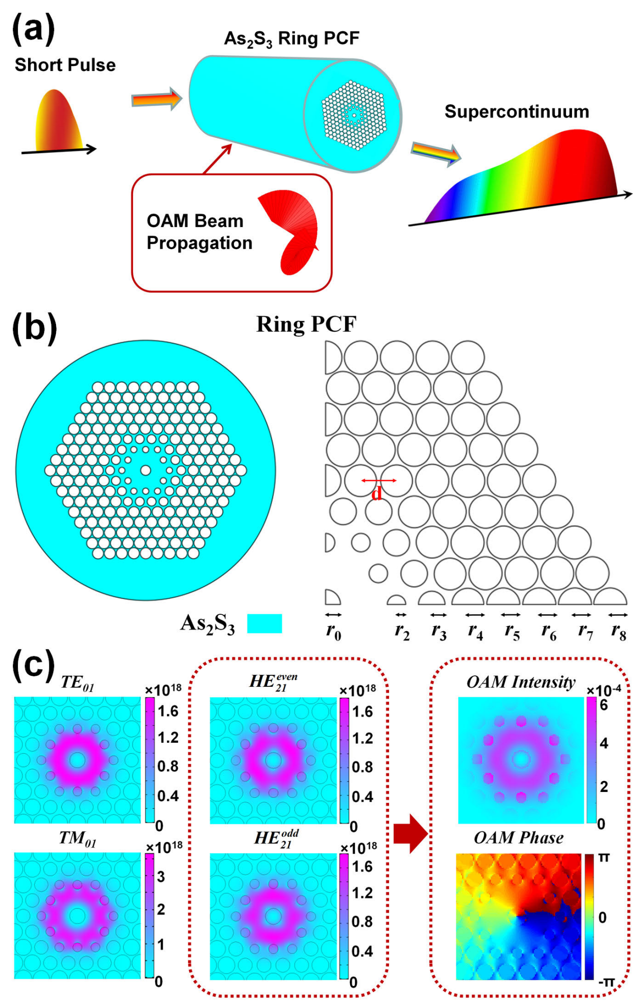

FIGURE 1. (a) The concept diagram of supercontinuum generation in the proposed As_2S_3 ring PCF. (b) Cross section of the designed ring-core As_2S_3 PCF. (c) The modal distribution of the fiber eigenmodes (TE_{01}, TM_{01}, $HE_{2,1}^{even}$ and $HE_{2,1}^{odd}$) and the corresponding OAM $_{1,1}$ mode ($OAM_{1,1} = HE_{2,1}^{even} + i \times HE_{2,1}^{odd}$).

III. SUPERCONTINUUM GENERATION OF $OAM_{1,1}$ IN PCF WITH ALL-NORMAL DISPERSION

A. FIBER PROPERTIES WITH OPTIMIZED DISPERSION

Figure 2(a) illustrates the chromatic dispersion of the $OAM_{1,1}$ mode in the As_2S_3 PCF with different r_3 (d = 0.4 μm, r_0 = 0.20 μm, r_2 = 0.1 μm, r_4 = 0.18 μm, r_5 to r_8 = 0.19 μm). To achieve all-normal and near-zero dispersion, we choose r_3 = 0.15 μm as the key parameter to the next step optimization. In order to get a flatter dispersion profile represented in Fig. 2(b), we further tailor the radius of the central air hole with d = 0.4 μm, r_2 = 0.1 μm, r_3 = 0.15 μm, r_4 = 0.18 μm, r_5 to r_8 = 0.19 μm. It can be seen that the dispersion curve of r_0 = 0.17 μm is all-normal and flat over a broad bandwidth. The maximum dispersion of the OAM mode in the proposed PCF is −36.5 ps/(nm·km) and its dispersion varies <60 ps/(nm·km) over a 940-nm bandwidth from 1740 to 2680 nm. At 1550 nm, the index difference between vortex modes (TE_{01}, TM_{01} and $OAM_{1,1}$) for the same structure parameters As_2S_3 PCF are all two-orders-of-magnitude larger than the value in the regular ring fiber ($\sim 10^{-4}$).

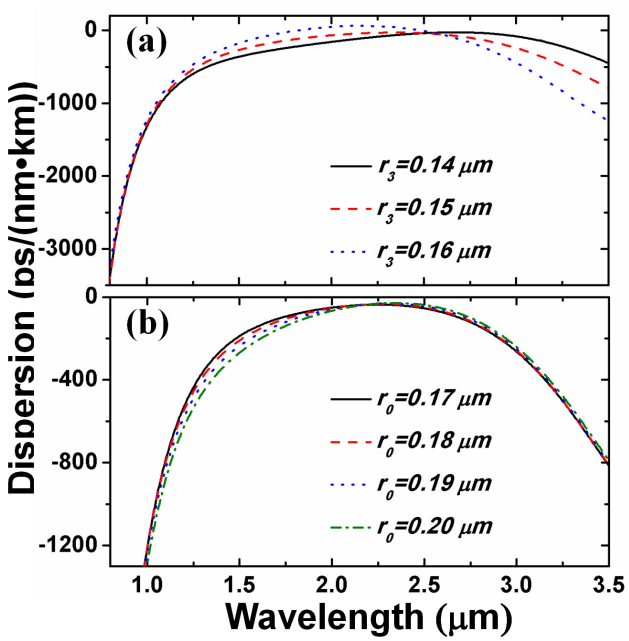

FIGURE 2. (a) Chromatic dispersion of the $OAM_{1,1}$ mode for different r_3. (b) Chromatic dispersion of the $OAM_{1,1}$ mode for different r_0.

The nonlinear coefficient γ and confinement loss of $OAM_{1,1}$ are displayed in Fig. 3. As the effective mode area increases with the wavelength, the nonlinear coefficient decreases and the confinement loss increases. At 2000 nm, the effective mode area of the OAM mode is 2.25 μm^2, and the corresponding large nonlinear coefficient is 4.55/W/m. The confinement loss is 1.04×10^{-4} dB/cm, which is relatively low.

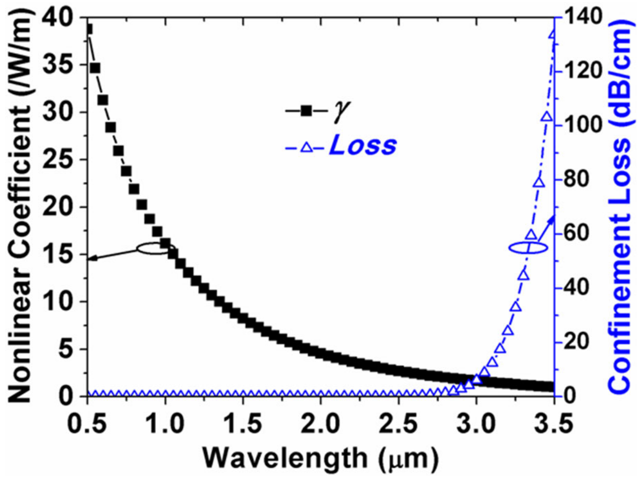

FIGURE 3. Nonlinear coefficient and confinement loss of $OAM_{1,1}$ mode in the optimized PCF.

The chromatic dispersion and nonlinear coefficient [27] of the mode supported in the proposed fiber is computed by the formula as follows:

$$D(\lambda) = \frac{-\lambda}{c}\frac{d^2 n_{eff}}{d\lambda^2} \tag{1}$$

$$A_{eff} = \frac{\left|\int (e_v \times h_v^*).\hat{z}\, dA\right|^2}{\int \left|(e_v \times h_v^*).\hat{z}\right|^2 dA} \tag{2}$$

$$\gamma = \frac{2\pi}{\lambda}\frac{\overline{n_2}}{A_{eff}} \tag{3}$$

where c represents the speed of the light in a vacuum, n_{eff} indicates the effective index of vortex modes as a function of the wavelength, A_{eff} is the effective mode area. The nonlinear refractive index n_2 of As_2S_3 is set as 3×10^{-18} m^2/W in our simulation [28].

B. FLAT AND COHERENT SC GENERATION

By using the split-step Fourier method and taking into consideration of the loss, dispersion, nonlinearity, and Raman effect [29], we further simulated the supercontinuum generation in the proposed PCF. A chirp-free hyperbolic secant pulse is launched into the optimized PCF. Because the transmission window of sulfide-based fiber is typically from 0.8 to 7 μm, the light could not propagate in the proposed fiber when the wavelength is below 800 nm. According to the experiment results of As_2S_3 PCFs [30], the loss is set to 0.4 dB/m in the wavelength range of 1000 to 2250 nm. From 800 nm, the loss is set as an exponential decay function towards 0.4 dB/m at 1000 nm [31]. For the wavelength range beyond 2250 nm, the confinement loss surpasses 0.4 dB/m, and thus the confinement loss is considered as the propagation loss. Overall, we used the worst possible loss across the spectral range simulated.

Figure 4(a) displays the effects of the peak power P of the input pulse on the supercontinuum after 10-mm fiber when the full width half maximum (FWHM) t_{FWHM} of the input pulse is 100 fs. The optical spectrum broadens prominently with the increase of the input pulse peak power. As indicated in Fig. 4(b), we change t_{FWHM} from 50 to 200 fs while P is set as 5 kW. With the t_{FWHM} of the input pulse decreasing, the flatness of the supercontinuum spectra gets better. Under the condition of constant peak power, the input pulse with larger t_{FWHM} has more energy and narrower spectra, which means each frequency component carrying more energy leads to stronger nonlinear effect [32]. To further investigate the influence of the pump wavelength on the SC generation, we change the center wavelength λ_0 from 1500 to 2500 nm, while keep P as 5 kW and t_{FWHM} as 100fs. Figure 4(c) illustrates that the SC spectra gradually moves towards the longer wavelength as λ_0 increases. Compared with the wavelength at 2000 nm, the SC is smoother when the input pulse pumps at 2500 nm. The spectrum is more fluctuated and the loss is larger as the wavelength increases.

Figure 5 describes the evolution of the supercontinuum along the As_2S_3 fiber, with a 100-fs 5-kW launched pulse. The optical spectrum is broadened along the propagation

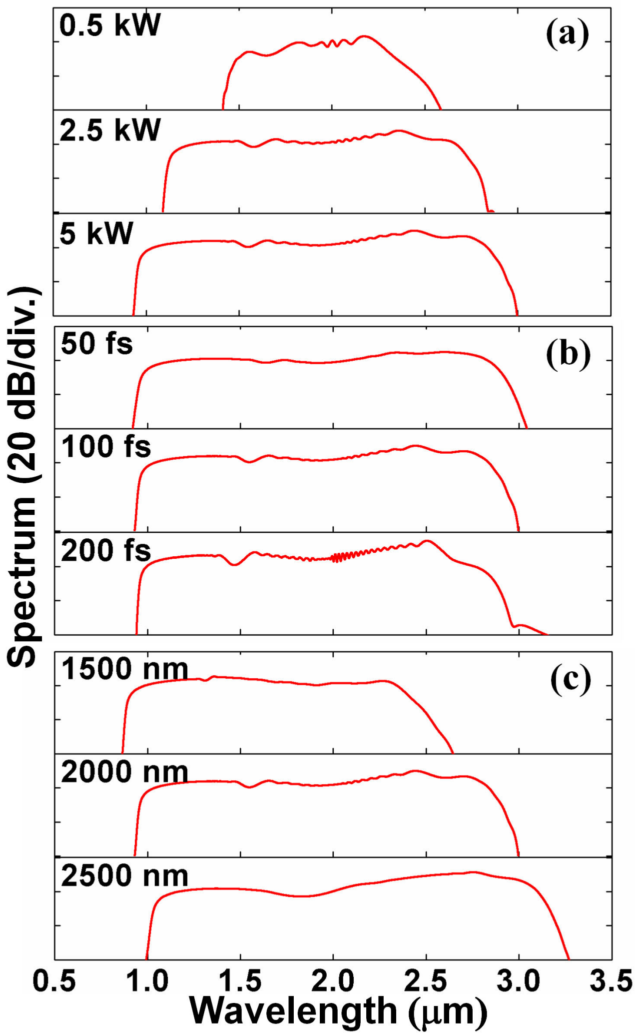

FIGURE 4. Influence of different input pulse parameters on SC generation of $OAM_{1,1}$ after the 10-mm long As_2S_3 ring PCF for different (a) peak power P (t_{FWHM} = 100 fs, λ_0 = 2000 nm), (b) pulse FWHM t_{FWHM} (P = 5 kW, λ_0 = 2000 nm), (c) central wavelength λ_0 (t_{FWHM} = 100 fs, P = 5 kW).

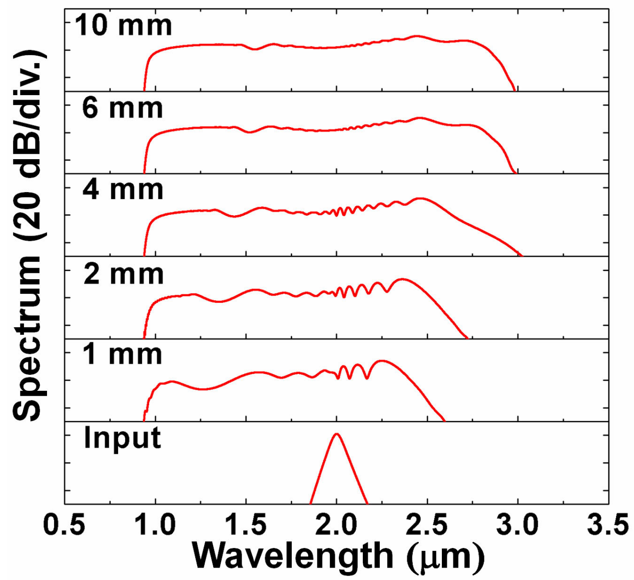

FIGURE 5. Octave-spanning $OAM_{1,1}$ supercontinuum generated along the proposed PCF (P = 5 kW, t_{FWHM} = 100 fs, λ_0 = 2000 nm) with different length.

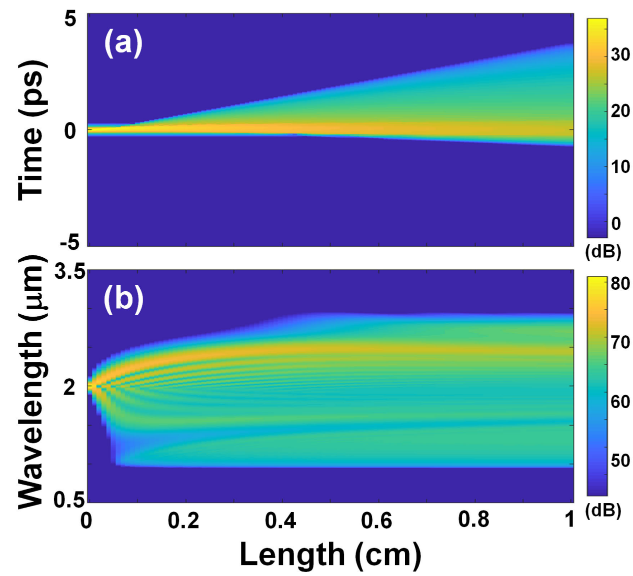

FIGURE 6. Temporal and spectral evolutions of the pump pulse along 10-mm As_2S_3 PCF (P = 5 kW, t_{FWHM} = 100 fs, λ_0 = 2000 nm).

length, and tends to be stable and flat at 10-mm length. After 10-mm propagation along the fiber, one can see that the input pulse with $P = 5$ kW, $t_{FWHM} = 100$ fs is already able to generate a flat and broad 1946-nm supercontinuum from 959 to 2905 nm at −20 dB, which covers 1.6-octave bandwidth. At −10 dB level, the supercontinuum can still cover >1.4 octave bandwidth from 1038 to 2837 nm.

Figure 6 represents the temporal and spectral evolutions of the pump pulses along the 1.0-cm As_2S_3 PCF. The principle of spectrum broadening in fiber with all-normal dispersion is self-phase modulation (SPM), self-steepening and optical wave breaking (OWB). The normal dispersion and SPM contribute to the initial temporal and spectral evolutions of the pump pulse. The red and blue frequency components are generated near the front and back edges, respectively. In this process, the peak power of the pulse decreases rapidly. Then, the new spectral components are generated because of OWB, which can be explained as a degenerate four-wave mixing (FWM). As the pulse continues to propagate after 0.1-cm fiber, the walk-off between the new components gets larger with the accumulated dispersion as identified in Fig. 6(a). The spectra are no longer broadened and become smooth after 0.5-cm propagation, as illustrated in Fig. 6(b).

IV. SUPERCONTINUUM GENERATION OF TE_{01} AND TM_{01} IN PCF WITH ALL-NORMAL DISPERSION

A. FIBER PROPERTIES WITH OPTIMIZED DISPERSION

To enable coherent supercontinuum generation of the other vortex modes in the proposed As_2S_3 ring PCF, we further

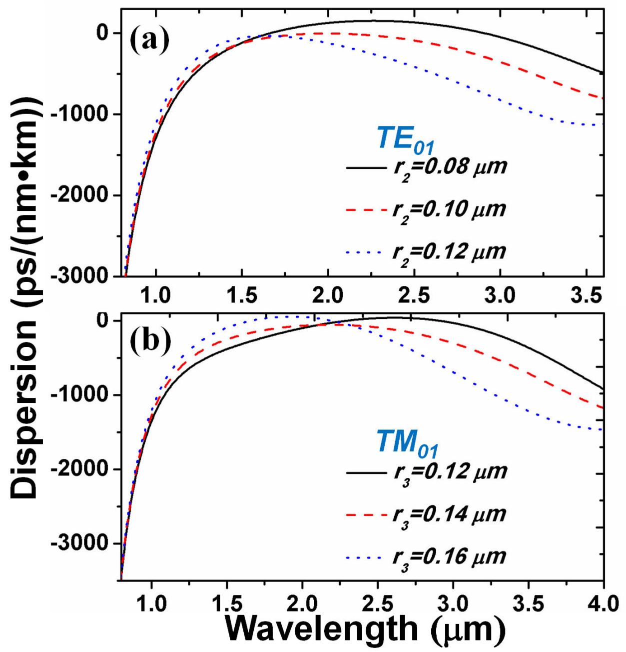

FIGURE 7. Chromatic dispersion of (a) the TE_{01} mode for different r_2, (b) the TM_{01} mode for different r_3.

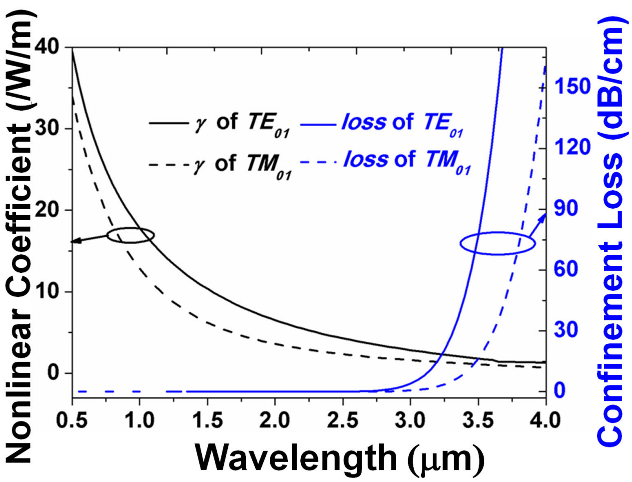

FIGURE 8. Nonlinear coefficient and confinement loss of the TE_{01} ($d = 0.4$ μm, $r_0 = 0.18$ μm, $r_2 = 0.1$ μm, $r_3 = 0.17$ μm, $r_4 = 0.18$ μm, r_5 to $r_8 = 0.19$ μm) and TM_{01} ($d = 0.4$ μm, $r_0 = 0.08$ μm, $r_2 = 0.08$ μm, $r_3 = 0.14$ μm, $r_4 = 0.18$ μm, r_5 to $r_8 = 0.19$ μm) modes in the optimized PCF structure parameters.

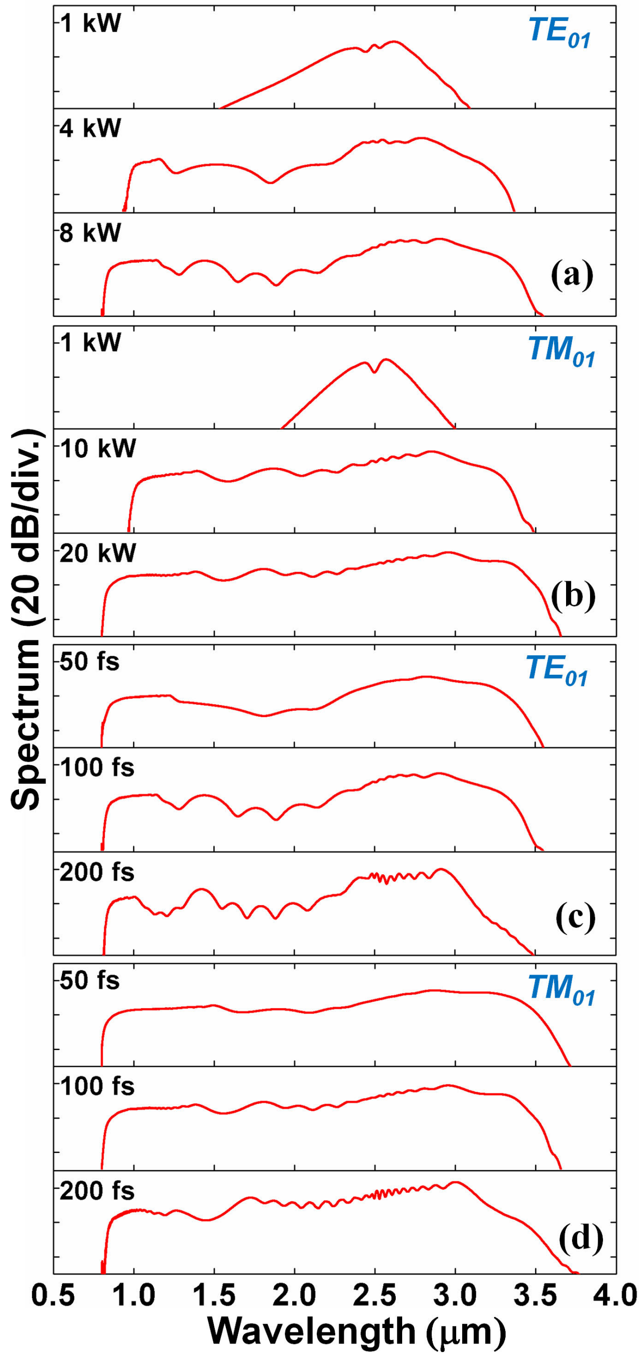

FIGURE 9. Effect of different input pulse parameters on the SC generation for TE_{01} and TM_{01} when the length of the As_2S_3 ring PCF is 2 mm (λ_0 =2500 nm): (a)-(b) peak power P when t_{FWHM} = 100 fs, (c)-(d) pulse FWHM t_{FWHM} when P = 8 kW for TE_{01} and P = 20 kW for TM_{01}.

optimized the geometric parameters to achieve all-normal and near-zero dispersion of the TE_{01} and TM_{01} modes. Figure 7(a) depicts the chromatic dispersion of the TE_{01} mode in the As_2S_3 PCF with r_2 varied from 0.08 μm to 0.12 μm ($d = 0.4$ μm, $r_0 = 0.18$ μm, $r_3 = 0.17$ μm, $r_4 = 0.18$ μm, r_5 to $r_8 = 0.19$ μm). As the diameter of the first ring of the cladding air hole increases, the dispersion curve at long wavelength region decreases significantly, while the dispersion slightly increases at the short wavelengths. The dispersion is flatter and near zero when $r_2 = 0.1$ μm. In the proposed PCF, the maximum dispersion of the TE_{01} mode is -3.8 ps/(nm·km). An average of -33.8 ps/(nm·km) dispersion is obtained with $< \pm 30$ ps/(nm·km) variation over a 794-nm bandwidth from 1624 to 2418 nm.

Figure 7(b) displays the dispersion profiles of the TM_{01} mode in the As_2S_3 PCF when r_3 varies from 0.12 μm to 0.16 μm ($d = 0.4$ μm, $r_0 = 0.08$ μm, $r_2 = 0.08$ μm,

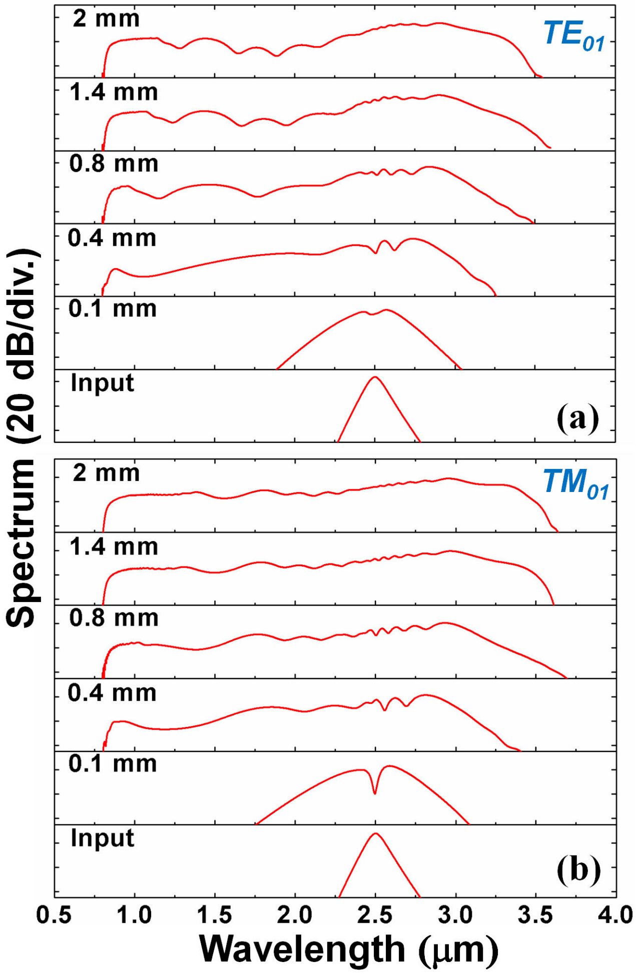

FIGURE 10. Octave-spanning supercontinuum of (a) the TE_{01} mode (P = 8 kW, t_{FWHM} = 100 fs, λ_0 = 2500 nm), and (b) the TM_{01} mode (P = 20 kW, t_{FWHM} = 100 fs, λ_0 = 2500 nm) generated along the proposed PCF, respectively.

r_4 = 0.18 μm, r_5 to r_8 = 0.19 μm). As one can observe in the figure, the chromatic dispersion at short wavelength region increases with increased r_3, but at longer wavelength the change is reversed. Therefore, the fiber with $r_3 = 0.14$ μm is selected to achieve all-normal and flatter dispersion. The dispersion varies between −96.1 and −56.1 ps/(nm·km) over a 660-nm bandwidth from 1855 to 2515 nm.

The nonlinear coefficient γ and confinement loss of the TE_{01} and TM_{01} modes under the optimized structure are depicted in Fig. 8. With the increased wavelength, the nonlinear coefficient decreases and the confinement loss increases. The wavelengths are 2286 nm and 2470 nm, when the confinement loss of the TE_{01} and TM_{01} modes surpasses 0.4 dB/m, respectively. At 2500 nm, the nonlinear coefficient γ of TE_{01} and TM_{01} are 4.30 and 2.36 /W/m. Here, their corresponding confinement losses are 0.05 and 0.006 dB/cm, respectively.

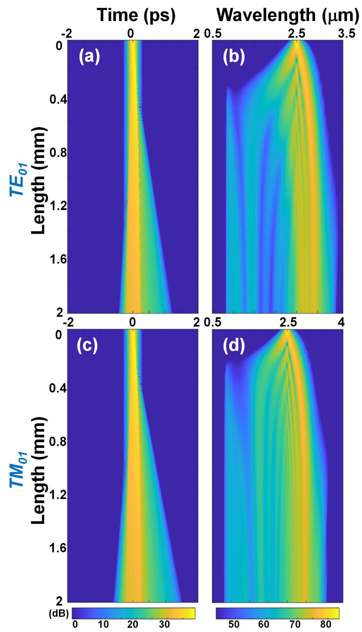

FIGURE 11. (a)–(c) Temporal and (b)-(d) spectral evolutions of the pump pulse with TE_{01} and TM_{01} modes propagating along the optimized PCF.

B. FLAT AND COHERENT SC GENERATION

Figure 9(a)-9(b) depicts the dependence of the supercontinuum spectra on the input pulse peak power P for TE_{01} and TM_{01} modes after 2-mm fiber, with the center pump wavelength of 2500 nm and the FWHM of 100 fs. The trend is similar as the OAM mode. As one can see in Fig 9, the supercontinuum broadens with the increasing of the peak power due to the stronger nonlinear effects. SPM and OWB effects will flat the SC spectrum until the peak power is saturated, thus the spectrum no longer broadens. As illustrated in Fig. 9(c)-9(d), we also analyze the effect of the input pulse FWHM on the spectra. With the decreased input pulse width, the generated supercontinuum becomes broader and smoother.

Figure 10 summarizes the supercontinua of the TE_{01} and TM_{01} modes propagate along the fiber. With the increased propagation length, the SC spectrum broadens and flattens due to SPM and OWB. The spectrum tends to be stable after 2-mm long propagation. A flat and broad SC spectrum of the TE_{01} mode is generated after 2-mm propagation with >2 octave bandwidth from 819 to 3440 nm at −30 dB. The supercontinuum of the TM_{01} mode is generated from 849 to 3504 nm at −20 dB. The spectral coverage of the TM_{01} supercontinuum is also >2 octave bandwidth. The loss of the TM_{01} mode, which is lower than that of the TE_{01} mode, contributes to its broadening at long wavelength range.

More details on the generation of supercontinuum are illustrated in Fig. 11. One can see the temporal and spectral evolutions of the pump pulses with the TE_{01} and TM_{01} modes propagating along the optimized PCF. The process of

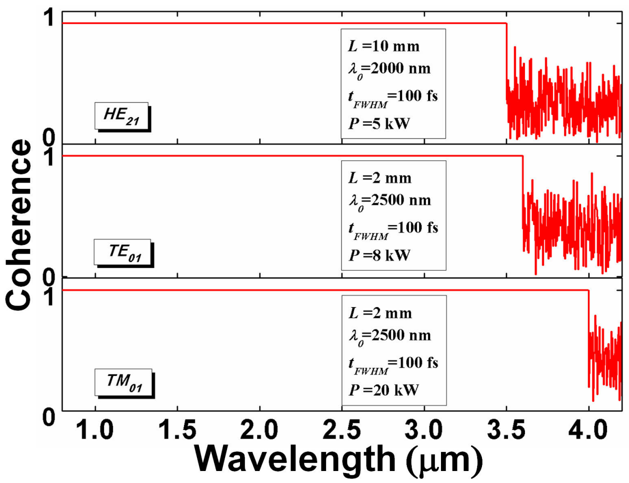

FIGURE 12. The coherence of HE_{21}, TE_{01} and TM_{01} modes generated supercontinuum (*L* represents the length of the fiber).

the SC generation is the same as the $OAM_{1,1}$ mode which is discussed in section III. The spectra are both broad and smooth after 2-mm propagation.

V. COHERENCE

Figure 12 illustrates the coherence of the generated supercontinua for different modes. Under the combined effects of the SPM and OWB processes, the SC generated in the all-normal dispersion PCF produces new spectra components, which has fixed phase difference compared with the input pulse. Therefore, the highly coherent SC spectrum can be achieved. This is difficult to be achieved for supercontinuum generated with anomalous dispersion where soliton dynamics effect dominates. In the simulation, we add one photon per mode Gaussian noise with a random phase to the input pulse for computing the coherence and execute 20 times. One can see that the coherence is 1 over the entire supercontinuum bandwidth for $OAM_{1,1}$, TE_{01}, and TM_{01} modes, respectively.

VI. CONCLUSION

In conclusion, we proposed an As_2S_3 ring-core PCF, which could guide vortex modes with all normal dispersion and high nonlinearity. By simulating the light guiding though the proposed fiber with different structure parameters, one can find the effect of these parameters on the chromatic dispersion. The all normal and flat dispersion of the $OAM_{1,1}$, TE_{01}, and TM_{01} modes is achieved by optimizing the PCF structure parameters, respectively. Simulations show that the designed fiber with all-normal dispersion could be used in highly coherent and broad supercontinuum generation because of SPM and OWB. With the dispersion varying from −96.5 to −36.5 ps/(nm·km) over a 940-nm bandwidth, the supercontinuum of the $OAM_{1,1}$ mode is generated from 959 to 2905 nm at −20 dB which covers a 1.6-octave bandwidth by launching a 100-fs 5-kW chirp-free hyperbolic secant pulse into a 1.0-cm designed fiber. The supercontinuum coverage of the TE_{01} and TM_{01} modes in the optimized fiber can both be over 2-octave bandwidth. The coherence of the generated supercontinuum of the three modes all shows nearly perfect property over the whole supercontinuum bandwidth.

REFERENCES

[1] N. Bozinovic, Y. Yue, Y. Ren, M. Tur, P. Kristensen, H. Huang, A. E. Willner, and S. Ramachandran, "Terabit-scale orbital angular momentum mode division multiplexing in fibers," *Science*, vol. 340, no. 6140, pp. 1545–1548, Jun. 2013.

[2] Y. Yue, Y. Yan, N. Ahmed, J.-Y. Yang, L. Zhang, Y. Ren, H. Huang, K. M. Birnbaum, B. I. Erkmen, S. Dolinar, M. Tur, and A. E. Willner, "Mode properties and propagation effects of optical orbital angular momentum (OAM) modes in a ring fiber," *IEEE Photon. J.*, vol. 4, no. 2, pp. 535–543, Apr. 2012.

[3] M. Sharma, P. Pradhan, and B. Ung, "Endlessly mono-radial annular core photonic crystal fiber for the broadband transmission and supercontinuum generation of vortex beams," *Sci. Rep.*, vol. 9, no. 2488, p. 2488, Feb. 2019.

[4] W. Yu, Z. Ji, D. Dong, X. Yang, Y. Xiao, Q. Gong, P. Xi, and K. Shi, "Super-resolution deep imaging with hollow bessel beam STED microscopy," *Laser Photon. Rev.*, vol. 10, no. 1, pp. 147–152, Jan. 2016.

[5] R. D. Niederriter, M. E. Siemens, and J. T. Gopinath, "Fiber optic sensors based on orbital angular momentum," in *Proc. Conf. Lasers Electro-Opt.*, 2015, pp. 1–2.

[6] M. Duocastella and C. B. Arnold, "Bessel and annular beams for materials processing," *Laser Photon. Rev.*, vol. 6, no. 5, pp. 607–621, Sep. 2012.

[7] L. Allen, M. W. Beijersbergen, R. J. C. Spreeuw, and J. P. Woerdman, "Orbital angular momentum of light and the transformation of Laguerre–Gaussian laser modes," *Phys. Rev. A, Gen. Phys.*, vol. 45, no. 11, pp. 8185–8189, Jun. 1992.

[8] H. Zhang, W. Zhang, L. Xi, X. Tang, X. Zhang, and X. Zhang, "A new type circular photonic crystal fiber for orbital angular momentum mode transmission," *IEEE Photon. Technol. Lett.*, vol. 28, no. 13, pp. 1426–1429, Jul. 1, 2016.

[9] C. Brunet, P. Vaity, Y. Messaddeq, S. LaRochelle, and L. A. Rusch, "Design, fabrication and validation of an OAM fiber supporting 36 states," *Opt. Express*, vol. 22, no. 21, pp. 26117–26127, 2014.

[10] S. Hong, Y. S. Lee, H. Choi, C. Quan, Y. Li, S. Kim, and K. Oh, "Hollow silica photonic crystal fiber guiding 101 orbital angular momentum modes without phase distortion in C+L band," *J. Lightw. Technol.*, vol. 38, no. 5, pp. 1010–1018, Mar. 1, 2020.

[11] P. S. J. Russell, "Nonlinear optics in photonic crystal fiber: Recent developments," in *Proc. Lasers Congr.*, 2016, Paper ATu5A.1.

[12] P. Russell, "Photonic crystal fibers," *Science*, vol. 299, no. 5605, pp. 358–362, 2003.

[13] P. Uebal, M. C. Günendi, M. H. Frosz, G. Ahmed, N. N. Edavalath, and J. Ménard, "Broadband robustly single-mode hollow-core PCF by resonant filtering of higher-order modes," *Opt. Lett.*, vol. 41, no. 9, pp. 1961–1964, May 2016.

[14] Y. Yue, G. Kai, Z. Wang, T. Sun, L. Jin, Y. Lu, C. Zhang, J. Liu, Y. Li, Y. Liu, S. Yuan, and X. Dong, "Highly birefringent elliptical-hole photonic crystal fiber with squeezed hexagonal lattice," *Opt. Lett.*, vol. 32, no. 5, pp. 469–471, Mar. 2007.

[15] T. Yang, E. Wang, H. Jiang, Z. Hu, and K. Xie, "High birefringence photonic crystal fiber with high nonlinearity and low confinement loss," *Opt. Express*, vol. 23, no. 7, pp. 8329–8337, Apr. 2015.

[16] B. K. Paul, M. Abdul Khalek, S. Chakma, and K. Ahmed, "Chalcogenide embedded quasi photonic crystal fiber for nonlinear optical applications," *Ceram. Int.*, vol. 44, no. 15, pp. 18955–18959, Oct. 2018.

[17] T. Schreiber, F. Röser, O. Schmidt, J. Limpert, R. Iliew, and F. Lederer, "Stress-induced single-polarization single-transverse mode photonic crystal fiber with low nonlinearity," *Opt. Express*, vol. 13, no. 19, pp. 7621–7630, Sep. 2005.

[18] C. Huang, M. Liao, W. Bi, X. Li, L. Hu, L. Zhang, L. Wang, G. Qin, T. Xue, D. Chen, and W. Gao, "Ultraflat, broadband, and highly coherent supercontinuum generation in all-solid microstructured optical fibers with all-normal dispersion," *Photon. Res.*, vol. 6, no. 6, pp. 601–608, Jun. 2018.

[19] G. Prabhakar, P. Gregg, L. Rishoj, P. Kristensen, and S. Ramachandran, "Octave-wide supercontinuum generation of light-carrying orbital angular momentum," *Opt. Express*, vol. 27, no. 8, pp. 11547–11556, Apr. 2019.

[20] D. Huang, E. A. Swanson, C. P. Lin, J. S. Schuman, W. G. Stinson, W. Chang, M. R. Hee, T. Flotte, K. Gregory, and C. A. Puliafito, "Optical coherence tomography," *Science*, vol. 254, no. 5035, pp. 1178–1181, Nov. 1991.
[21] M. Tsuzuki, L. Jin, M. Yamanaka, V. Sonnenchein, H. Tomita, A. Sato, T. Ohara, Y. Sakaibara, E. Omoda, H. Kataura, T. Iguchi, and N. Nishizawa, "Midinfrared optical frequency comb based on difference frequency generation using high repetition rate Er-doped fiber laser with single wall carbon nanotube film," *Photon. Res.*, vol. 4, no. 6, pp. 313–317, Dec. 2016.
[22] B. J. Eggleton, B. Luther-Davies, and K. Richardson, "Chalcogenide photonics," *Nature Photon.*, vol. 5, no. 3, pp. 141–148, Feb. 2011.
[23] Y. Yue, L. Zhang, Y. Yan, N. Ahmed, J. Yang, H. Huang, Y. Ren, S. Dolinar, M. Tur, and A. E. Willner, "Octave-spanning supercontinuum generation of vortices in an As_2S_3 ring photonic crystal fiber," *Opt. Lett.*, vol. 37, no. 11, pp. 1889–1891, Jun. 2012.
[24] A. M. Heidt, A. Hartung, G. W. Bosman, P. Krok, E. G. Rohwer, H. Schwoerer, and H. Bartelt, "Coherent octave spanning near-infrared and visible supercontinuum generation in all-normal dispersion photonic crystal fibers," *Opt. Express*, vol. 19, no. 4, pp. 3775–3787, Feb. 2011.
[25] L. E. Hooper, P. J. Mosley, A. C. Muir, W. J. Wadsworth, and J. C. Knight, "Coherent supercontinuum generation in photonic crystal fiber with all-normal group velocity dispersion," *Opt. Express*, vol. 19, no. 6, pp. 4902–4907, 2011.
[26] J. M. Dudley, G. Genty, and S. Coen, "Supercontinuum generation in photonic crystal fiber," *Rev. Modern Phys.*, vol. 78, no. 4, pp. 1135–1184, 2006.
[27] S. Afshar and T. M. Monro, "A full vectorial model for pulse propagation in emerging waveguides with subwavelength structures part I: Kerr nonlinearity," *Opt. Express*, vol. 17, no. 4, pp. 2298–2318, 2009.
[28] L. Zhang, Y. Yue, Y. Xiao-Li, J. Wang, R. G. Beausoleil, and A. E. Willner, "Flat and low dispersion in highly nonlinear slot waveguides," *Opt. Express*, vol. 18, no. 12, pp. 13187–13193, Jun. 2010.
[29] W. Gao, M. E. Amraoui, M. Liao, H. Kawashima, Z. Duan, D. Deng, T. Cheng, T. Suzuki, Y. Messaddeq, and Y. Ohishi, "Mid-infrared supercontinuum generation in a suspended-core As_2S_3 chalcogenide microstructured optical fiber," *Opt. Express*, vol. 21, no. 8, pp. 9573–9583, Apr. 2013.
[30] M. El-Amraoui, J. Fatome, J. C. Jules, B. Kibler, G. Gadret, C. Fortier, F. Smektala, I. Skripatchev, C. F. Polacchini, Y. Messaddeq, J. Troles, L. Brilland, M. Szpulak, and G. Renversez, "Strong infrared spectral broadening in low-loss As-S chalcogenide suspended core microstructured optical fibers," *Opt. Express*, vol. 18, no. 5, pp. 4547–4556, Mar. 2010.
[31] A. Zakery, Y. Ruan, A. V. Rode, M. Samoc, and B. Luther-Davies, "Low-loss waveguides in ultrafast laser-deposited As_2S_3 chalcogenide films," *J. Opt. Soc. Amer. B, Opt. Phys.*, vol. 20, no. 9, pp. 1844–1852, Sep. 2003.
[32] Y. Fang, C. Bao, Z. Wang, B. Liu, L. Zhang, X. Han, Y. He, H. Huang, Y. Ren, Z. Pan, and Y. Yue, "Three-octave supercontinuum generation using SiO_2 cladded Si_3N_4 slot waveguide with all-normal dispersion," *J. Lightw. Technol.*, vol. 38, no. 13, pp. 3431–3438, Jul. 1, 2020.

WENPU GENG received the B.S. degree in optical information science and technology from Nankai University, Tianjin, China, in 2019, where she is currently pursuing the M.S. degree in optical engineering with the Institute of Modern Optics.

CHANGJING BAO (Member, IEEE) received the Ph.D. degree in electrical engineering from the University of Southern California, Los Angeles, CA, USA, in 2017. He has authored or coauthored more than 100 journal articles and conference proceedings. His research interests include optical communications, nonlinear optics, and integrated optics.

YUXI FANG received the B.S. degree in optical information science and technology from Anhui University, Hefei, China, in 2018. She is currently pursuing the master's degree with the Institute of Modern Optics, Nankai University, Tianjin, China. Her research interest includes integrated optics.

YINGNING WANG received the B.S. degree in electronic science and technology from Shandong University, Qingdao, China, in 2019. She is currently pursuing the M.S. degree in optical engineering with the Institute of Modern Optics, Nankai University, Tianjin, China.

YIQIAO LI is currently pursuing the B.S. degree in communication engineering with Nankai University, Tianjin, China.

ZHI WANG received the Ph.D. degree in optics from Nankai University, Tianjin, China, in 2005. He is currently a Professor with the Institute of Modern Optics, Nankai University. His research interests include photonic crystal fibers/multimode fiber mode control theory, micro/nanostructured fiber sensing technology, ultrafast fiber laser technology, nonlinear fiber optics, and the nonlinear space-time dynamics of multimode fibers.

YAN-GE LIU received the M.S. degree in optics from Nankai University, Tianjin, China, in 1998, and the Ph.D. degree in optics engineering from Tianjin University, Tianjin, in 2001.

She is currently a Professor with the Institute of Modern Optics, Nankai University. She has published more than 130 peer-reviewed journal articles with total citations of more than 2000 times. Her research interests include micro/nanostructured optical fiber devices, optical fiber communication and sensing technology, and optical fiber lasers and amplifiers.

HAO HUANG (Member, IEEE) received the B.S. degree from Jilin University, Changchun, China, in 2006, the M.S. degree from the Beijing University of Posts and Telecommunications, Beijing, China, in 2009, and the Ph.D. degree in electrical engineering from the University of Southern California, Los Angeles, CA, USA, in 2014. He is currently working as a Hardware Engineer with Lumentum Operations LLC. He has coauthored more than 100 publications, including peer-reviewed journals and conference proceedings. His research interests include optical communication system and components, optical sensing systems, and digital signal processing. He is a member of the Optical Society of America (OSA).

YONGXIONG REN (Member, IEEE) received the B.E. degree in communications engineering from the Beijing University of Posts and Telecommunications (BUPT), Beijing, China, in 2008, the M.S. degree in radio physics from Peking University (PKU), Beijing, in 2011, and the Ph.D. degree in electrical engineering from the University of Southern California (USC), Los Angeles, CA, USA, in 2016.

His publications include 57 peer-reviewed journal articles, 76 international conference proceedings, one book chapter, and holds three patents. He has authored or coauthored more than 130 research articles with a Google Scholar citation number of more than 5500. His main research interests include high-capacity free-space and fiber optical communications, millimeter-wave communications, space division multiplexing, orbital angular momentum multiplexing, atmospheric optics, and atmospheric turbulence compensation.

ZHONGQI PAN (Senior Member, IEEE) received the B.S. and M.S. degrees from Tsinghua University, China, and the Ph.D. degree from the University of Southern California, Los Angeles, all in electrical engineering.

He is currently a Professor with the Department of Electrical and Computer Engineering, University of Louisiana at Lafayette. He also holds BORSF Endowed Professorship in Electrical Engineering II and the BellSouth/BORSF Endowed Professorship in Telecommunications. His research interests include the area photonics, including photonic devices, fiber communications, wavelength-division-multiplexing (WDM) technologies, optical performance monitoring, coherent optical communications, space-division-multiplexing (SDM) technologies, and fiber sensor technologies. He has authored or coauthored 160 publications, including five book chapters and 18 invited presentations/articles. He also holds five U.S. patents and one China patent. He is a Senior Member of the Optical Society of America (OSA).

YANG YUE (Member, IEEE) received the B.S. and M.S. degrees in electrical engineering and optics from Nankai University, Tianjin, China, in 2004 and 2007, respectively, and the Ph.D. degree in electrical engineering from the University of Southern California, Los Angeles, CA, USA, in 2012.

He is a Professor with the Institute of Modern Optics, Nankai University. He has published over 170 peer-reviewed journal articles and conference proceedings, three edited books, one book chapter, more than ten invited articles, more than 80 invited presentations, and holds more than 30 issued or pending patents. His current research interests include intelligent photonics, optical communications and networking, optical interconnect, detection, imaging, and display technologies, integrated photonics, and free-space and fiber optics.

Dr. Yue is a member of the IEEE Communications Society (ComSoc), the IEEE Photonics Society (IPS), the International Society for Optical Engineering (SPIE), the Optical Society of America (OSA), and the Photonics Society of Chinese–American (PSC). He also served as guest editor for seven journal special issues, a committee member, and the session chair for 30 international conferences, and a reviewer for more than 50 prestigious journals and OSA Centennial Special Events Grant in 2016. He is an Associate Editor of IEEE ACCESS and an editorial board member of three other scientific journals.